Article

Impact of the Flavonoid Quercetin on β-Amyloid Aggregation Revealed by Intrinsic Fluorescence

Abeer Alghamdi, David J.S. Birch, Vladislav Vyshemirsky, and Olaf J. Rolinski*

Read Online

ACCESS | Metrics & More | Article Recommendations | Supporting Information

ABSTRACT: We report the effects of quercetin, a flavonoid present in the human diet, on early stage beta-amyloid (Aβ) aggregation, a seminal event in Alzheimer's disease. Molecular level changes in Aβ arrangements are monitored by time-resolved emission spectral (TRES) measurements of the fluorescence of Aβ's single tyrosine intrinsic fluorophore (Tyr). The results suggest that quercetin binds β-amyloid oligomers at early stages of their aggregation, which leads to the formation of modified oligomers and hinders the creation of β-sheet structures, potentially preventing the onset of Alzheimer's disease.
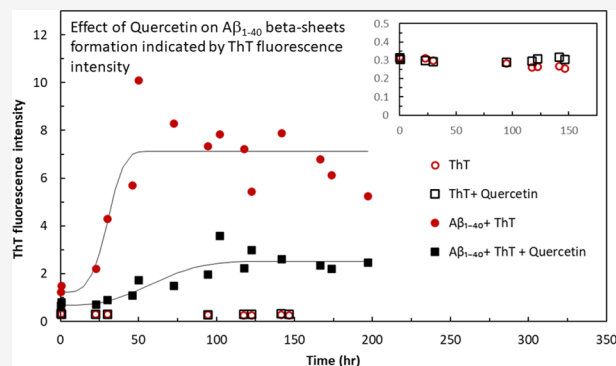
INTRODUCTION

Flavonoids consist of a large group of polyphenolic compounds having a benzo-γ-pyrone structure and are ubiquitous in plants. To date, more than 8000 varieties of flavonoids have been identified.[1,2] One important subclass of flavonoids, the flavonols and their major representative quercetin, are the most prevalent flavonoids in the human diet.[3−5] They occur in many vegetables and fruits such as onions, curly kale, broccoli, blueberries, and apples as well as in red wine, tea, and cocoa.

Quercetin has gained much scientific attention due to its antioxidant and metal ion-chelating properties[6−9] and its capacity to inhibit amyloid fibril formation.[10] Many human neurodegenerative diseases such as Alzheimer's and Parkinson's disease are associated with amyloid fibril formation; thus, quercetin is intensively researched for its therapeutic potential in providing improved treatment for neurodegenerative diseases.

Alzheimer's disease (AD) is the most common progressive neurodegenerative disease and one of the leading causes of dementia globally.[11] The two major pathological hallmarks of AD are extracellular β-amyloid (Aβ) plaques and intracellular τ-containing neurofibrillary tangles. The prevailing view of AD pathogenesis today[12−17] is that accumulation of Aβ either as oligomers or fibrils initiates a pathophysiological cascade resulting in τ misfolding and aggregation that spreads throughout the brain, eventually leading to neural system failure and cognitive decline. This clearly implicates Aβ as a critical disease initiator. Consequently, most of the attention in the scientific community has focused on ways to reduce Aβ production, inhibit aggregation, increase removal, and identify the toxic amyloid forms.

Quercetin has been reported to exert antioxidant activity due to the catechol group in the β ring and the OH group located in positions 3 and 5 of the AC ring[18] (Figure 1a). It is also suggested that quercetin might indirectly inhibit the formation of Aβ peptides by constraining the activity of the β-site APP cleaving enzyme (BACE-1).[19] Studies have shown that OH groups and phenolic rings in flavonoids are essential for the noncovalent interactions with β-sheet structures, which are common to all amyloid proteins.[20] Studies on quercetin in particular have pointed out that it has the potential to inhibit Aβ aggregation by forming hydrophobic interactions and hydrogen bonds with the formed β-sheets.[19] More interestingly, it has been reported that quercetin has the ability to destabilize preformed fibrils in some proteins such as bovine insulin,[21] α-synuclein,[22] and A$\beta_{25−35}$[23] in a dose-dependent manner whereupon fibrils are transformed into amorphous aggregates.[21] The final morphologies of protein assemblies in the presence of quercetin are different and require further examination for better characterization.

In this research, we have used the intrinsic fluorescence of A$\beta_{1−40}$ peptides to study their oligomerization under the influence of quercetin. For a broader and more comprehensive understanding of the changes observed in the intrinsic Tyr$_{10}$ fluorescence intensity decay, we measured time-resolved

A
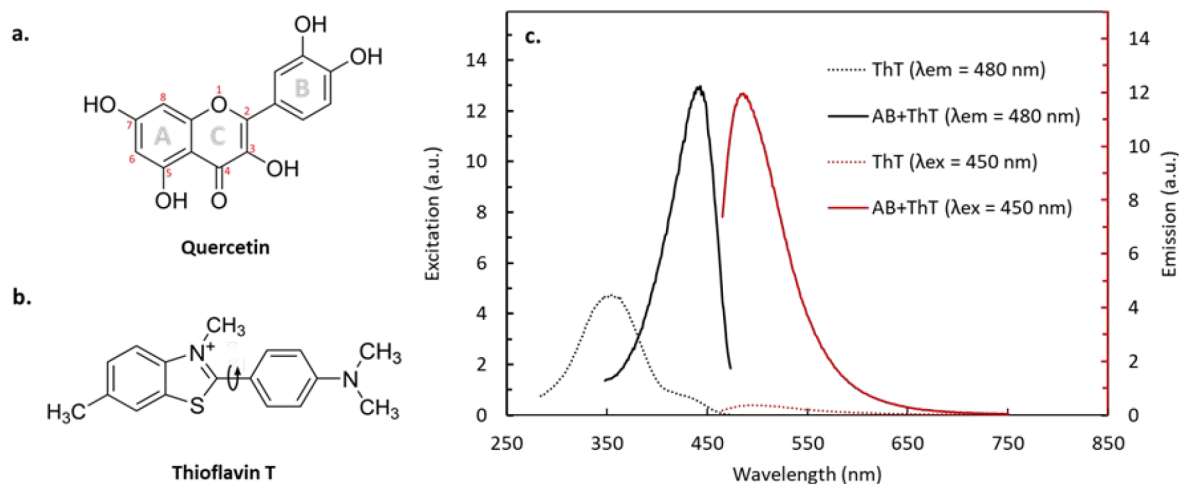
Figure 1. Chemical structure of quercetin (a) and thioflavin T (b). Fluorescence excitation (black) and emission (red) spectra of equal concentrations of ThT alone in HEPES buffer (dotted line) and ThT with $A\beta_{1-40}$ in the same buffer (solid line) measured after 72 h of incubation (c).

emission spectra (TRES), which can sufficiently demonstrate structural changes in $A\beta_{1-40}$, including aggregation, as we have shown in previous studies.[24]

To identify the direct effects of quercetin on Tyr_{10} in $A\beta_{1-40}$, which can be observed when the aggregation does not occur, we extended the lifetime measurements to the shorter fragments of the $A\beta_{1-40}$ peptide, such as $A\beta_{1-11}$ and $A\beta_{1-16}$. These peptides also contain the single Tyr residue but lack the hydrophobic C-terminal of $A\beta_{1-40}$, which is critical in triggering the transformation from the α-helical to β-sheet structure and plays a key role in aggregation.[25]

Further stages of $A\beta_{1-40}$ fibril formation followed by oligomerization were monitored by the thioflavin T (ThT) binding assay (Figure 1b). ThT is currently considered the gold-standard fluorescent probe for the study of amyloid fibril formation. Upon binding to β-sheet-rich structures, ThT gives a strong fluorescence signal at 482 nm when excited at 450 nm. The mechanism by which ThT fluorescence is enhanced upon binding to amyloids has been ascribed to the rotational immobilization of the C−C bond between the benzothiazole and aniline rings[26,27] (Figure 1b), which results in a dramatic shift in the ThT excitation maximum from 350 to 450 nm as shown in Figure 1c. Although ThT is an efficient reporter of fibril formation, its poor photophysical and binding properties make it ill-suited for detection of the small oligomeric species[28] that are critical precursors to fibril formation. Thus, the ThT assay is used here as a complementary technique, to confirm the formation of $A\beta_{1-40}$ fibrils.

EXPERIMENTAL SECTION

Sample Preparation. The lyophilized $A\beta_{1-40}$ powder ($A\beta_{1-40}$; Sigma-Aldrich, UK) was treated before use with 1,1,1,3,3,3- hexafluoro-2-propanol (HFIP; Sigma-Aldrich, UK). This procedure is routinely used[29,30] to ensure that the starting sample comprises only monomers. $A\beta_{1-40}$ was diluted in 100% HFIP to 0.1 mM and sonicated for 10 min. The clear solution containing the dissolved peptide was then aliquoted in Eppendorf microcentrifuge tubes, and the HFIP was allowed to evaporate in a fume hood. The samples were then stored at −20 °C.

Upon usage, the film of $A\beta_{1-40}$ was dissolved in 1% NH4OH at a concentration of 1 mg/mL, and this was sonicated for 30 s to 1 min. To prepare the free $A\beta_{1-40}$ sample, the solution was

diluted in 4-(2-hydroxyethyl)-1-piperazineethanesulfonic acid (HEPES; Sigma-Aldrich, UK, pH 7.4, 0.1 M) to a concentration of 50 μM. To prepare $A\beta_{1-40}$ samples with quercetin, a HEPES buffer containing quercetin dihydrate ($C_{15}H_{10}O_7\cdot2H_2O$; Riedel-de Haen, Germany) was added. The final concentrations of components in the sample were 50 μM $A\beta_{1-40}$ and 15 or 50 μM quercetin. For the ThT assay, a HEPES buffer containing ThT (Sigma-Aldrich, UK) with and without quercetin was added. The final concentrations of components in the sample were 50 μM $A\beta_{1-40}$, 15 μM ThT, and 15 or 50 μM quercetin. All $A\beta_{1-40}$ samples were incubated at a temperature of 36 °C over the entire time of the experiment.

$A\beta_{1-11}$ and $A\beta_{1-16}$ samples were prepared by dissolving $A\beta_{1-11}$ and $A\beta_{1-16}$ peptides ($A\beta_{1-11}/A\beta_{1-16}$; Sigma-Aldrich, UK) in 0.1 M HEPES to a concentration of 50 μM. Different concentrations of quercetin dihydrate (concentrations from 0 to 200 μM) were added to the solutions.

Steady-State Measurements. Steady-state fluorescence spectra of ThT and tyrosine in $A\beta_{1-11}$, $A\beta_{1-16}$, and $A\beta_{1-40}$ were obtained using a Fluorolog-3 spectrofluorimeter. The excitation and emission monochromators were set at 5 nm slit widths. Tyr was excited at 279 nm, and emission spectra were recorded at 290−500 nm in 1 nm increments. Measurements were repeated for the $A\beta_{1-40}$ sample at different times: 1, 24, 50/72, and 140 h after sample preparation. ThT was excited at 450 nm, and the emission spectra were recorded from 465 to 600 nm over a 200 h time period.

Time-Correlated Single Photon Counting (TCSPC). TCSPC measurements were conducted on a HORIBA Scientific DeltaFlex fluorometer (HORIBA Jobin Yvon IBH Ltd., Glasgow, UK). The system was equipped with Seya-Namioka monochromators with a focal length of 100 mm and a peak transmission efficiency of 62% for excitation and emission. Typical spectral bandwidths were 16 nm. The DeltaFlex system uses a HORIBA PPD photon counting detector (PPD-650), and a HORIBA NanoLED for excitation with a center wavelength of 279 nm, a pulse duration of 50 ps, and a repetition rate of 1 MHz.[31]

Fluorescence decay curves were obtained for $A\beta_{1-11}$ and $A\beta_{1-16}$ in the absence and presence of different concentrations of quercetin (25, 50, and 200 μM) at an emission wavelength of 316 nm.
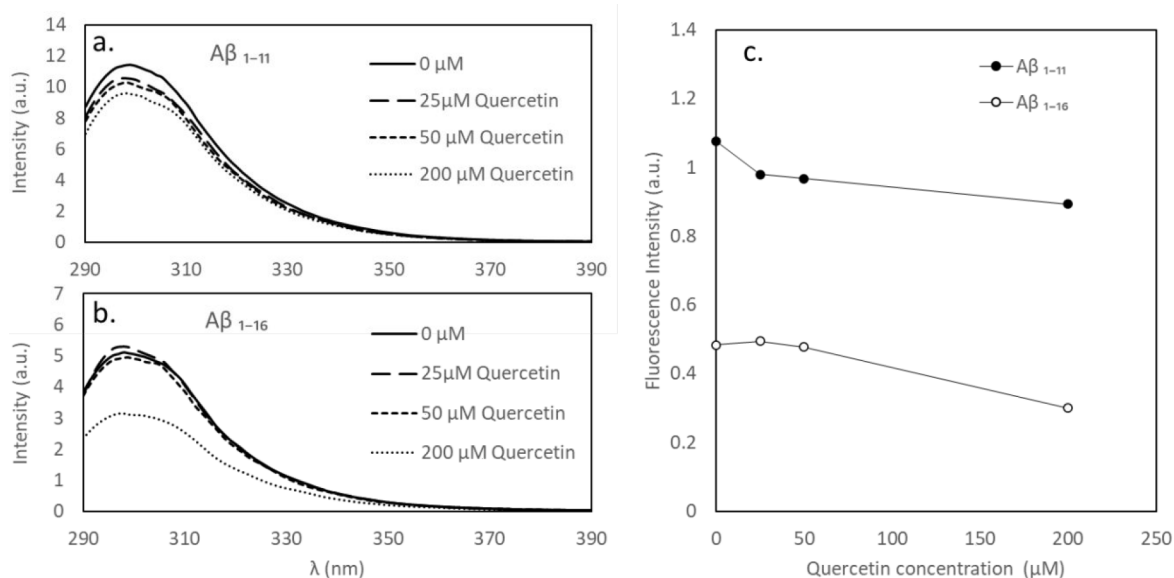
Figure 2. Emission spectra of $A\beta_{1-11}$ (a) and $A\beta_{1-16}$ (b) at excitation wavelength 279 nm in the absence (solid line) and presence of 25 μM (long dash), 50 μM (short dash), and 200 μM (dotted) quercetin. Maximum fluorescence intensity of $A\beta_{1-11}$ (black circle) and $A\beta_{1-16}$ (white circle) as a function of quercetin concentration (c).

For the $A\beta_{1-40}$ TRES measurements, a series of 12 fluorescence decay curves were collected at the emission wavelengths between 297 and 330 at 3 nm increments. Figure S1 in Supporting Information (SI) shows an example of three fluorescence decays measured at different stages of aggregation (1, 24, and 140 h) for free $A\beta_{1-40}$ and $A\beta_{1-40}$ with quercetin at concentrations 15 and 50 μM.

Fluorescence decay curves were analyzed using DAS6 reconvolution software that assumes that the experimental curve $F(t)$ directly accounts for the presence of scattered excitation light in the Tyr decay[32]

$$F(t) = a + bL(t + \Delta) + c \int_0^t L(t + \Delta - t')I(t') \, \mathrm{d}t' \tag{1}$$

where $L(t)$ is the prompt excitation function, and a, b, and c are the background noise level, contribution of the scattered light, and the scaling parameter, respectively. Δ approximates the effect of the time-shift between the prompt and decay curves due to the transit time wavelength dependence of the photomultiplier detector. $I(t)$ is the n-exponential model function. The recovered parameters of $I(t)$ were used in the TRES analysis.

Calculating Time-Resolved Emission Spectra (TRES). The reason why we decided to use the TRES approach, instead of applying the fluorescence intensity decay analysis based on a measurement at a single wavelength, was the previously observed[24,33] complexity of the fluorescence kinetics of $A\beta_{1-40}$, where the decay of the population of excited molecules is combined with the shifts in the transient emission spectra caused by dielectric relaxation. The TRES approach allows the resolution of these two processes. The fluorescence decays $I_\lambda(t)$, measured at individual wavelengths λ (see Figure S1 in SI), were fitted to multiexponential functions and then used to calculate the TRES $I_t(\lambda)$ from the equation

$$I_t(\lambda) = I_\lambda(t) \times \frac{S(\lambda)}{\int_0^\infty I_\lambda(t) \, \mathrm{d}t} \tag{2}$$

where $S(\lambda)$ is the steady-state fluorescence spectrum of the sample, and the integral is proportional to the total emitted photons in the lifetime experiment. The obtained spectra were then converted from the wavelength $I_t(\lambda)$ to the wavenumber scale according to $I_t(\nu) = \lambda^2 I_t(\lambda)$.

TRES were obtained for $A\beta_{1-40}$ at several stages of aggregation, namely, 1, 24, 50 or 72, and 140 h after sample preparation (the number indicates the age of the sample when the measurement at the first wavelength has been started). From the data obtained for each stage of aggregation, 14 TRES were calculated at different times after excitation. Figure S2 shows the TRES of samples in the absence and presence of 15 and 50 μM quercetin at different stages of aggregation (i.e., 1, 24, 50 or 72, and 140 h).

According to Toptygin and Brand,[34] the fluorescence spectrum of a single fluorescent residue can be expressed as $\sim \nu^3 g(\nu)$, where $g(\nu)$ is the Gaussian distribution function. Therefore, for the purpose of detailed analysis of the $A\beta_{1-40}$ TRES, we modeled the recovered spectra $I_t(\nu)$ at the time t as the sum of N components of the type $\sim \nu^3 g(\nu)$

$$I_t(\nu) = \sum_{i=1}^N \frac{C_i(t)\nu^3 \exp[-(\nu - \nu_i(t))^2 / (2\sigma_i^2(t))]}{\sqrt{2\pi}\nu_i(t)\sigma_i(t)(\nu_i^2(t) + 3\sigma_i^2(t))} \tag{3}$$

where t is the time after excitation in ns, ν is the wavenumber in cm^{-1}, $\sigma_i(t)$ is the standard deviation of each component, $\nu_i(t)$ is its peak position, and $C_i(t)$ is the fluorescence intensity contribution of the ith component at the time t, i.e., the fluorescence intensity decay of this component.

The obtained experimental TRES for the sample with and without quercetin demonstrated the presence of two components ($N = 2$). The parameters recovered from fitting the proposed model (eq 3 for $N = 2$) to the experimental data were used to analyze and compare the fluorescence kinetics of both samples.

In the presence of dielectric relaxation, $\nu_i(t)$ decays exponentially from a great value to a minimum value. To obtain the time of relaxation (τ_R), $\nu_i(t)$ decays were fitted to the equation
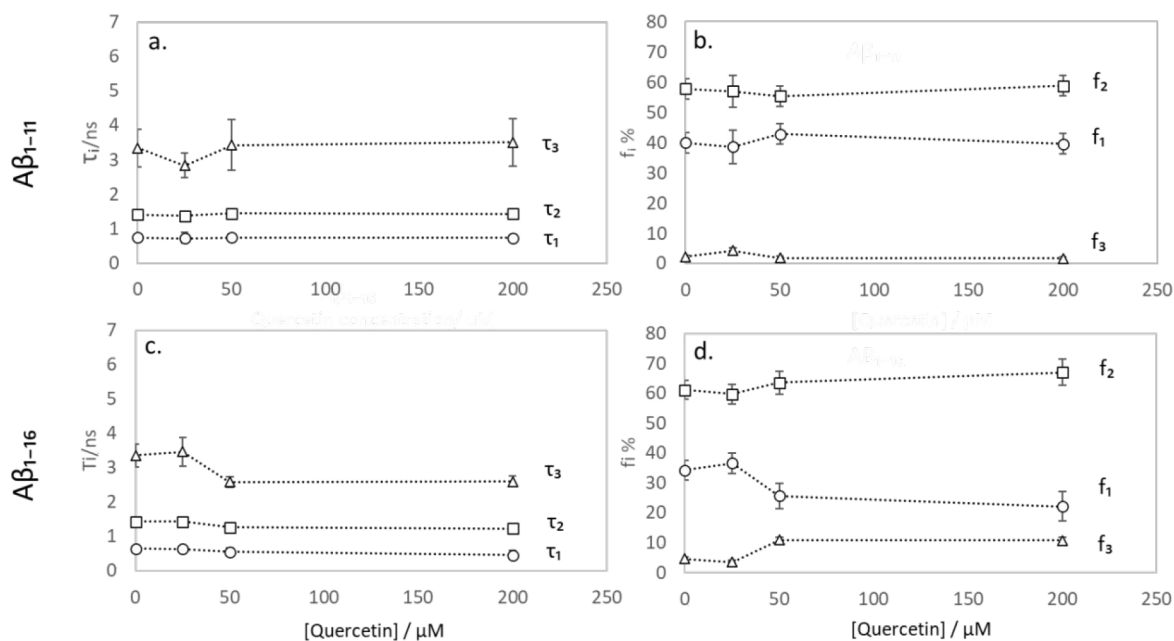
Figure 3. Parameters obtained from fitting Tyr's fluorescence decay in a 50 μM Aβ_{1-11} (a, b) and Aβ_{1-16} (c, d) solution at emission wavelength 316 nm to a three-exponential decay model plotted against quercetin concentration: Tyr fluorescence decay times τ_1, τ_2 and τ_3 in Aβ_{1-11} (a) and Aβ_{1-16} (c), percentage contributions f_1, f_2, and f_3 in Aβ_{1-11} (b) and Aβ_{1-16} (d). Error bars represent 3 × standard deviation.
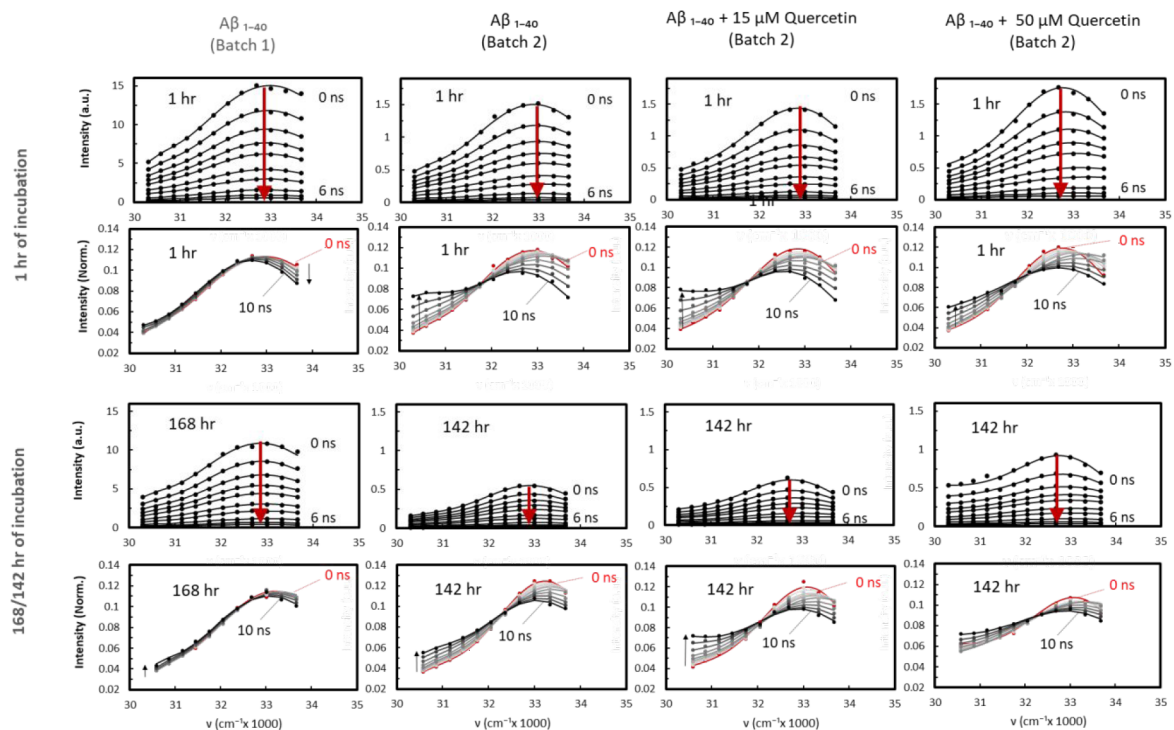
Figure 4. Time-resolved emission spectra (TRES) obtained for 50 μM Aβ_{1-40} in HEPES buffer (pH 7.4) in the absence (batch 1 and 2) and presence of two different concentrations of quercetin 15 and 50 μM (batch 2) after 1 h of incubation and 142/168 h of incubation. The solid lines represent the two-Toptygin-type function fits.

$$\nu_i(t) = \nu_\infty + (\nu_0 - \nu_\infty)e^{-t/\tau_R}$$

where ν_0 and ν_∞ are the position of the peak at $t = 0$ and $t = \infty$,

respectively.

RESULTS AND DISCUSSION

Aβ_{1-11} and Aβ_{1-16} Samples. Steady-state results show that increasing the concentration of quercetin up to 200 μM in a 50 μM Aβ_{1-11} sample slightly reduces the intensity of Tyr emission (Figure 2a). The emission of the 50 μM Aβ_{1-16} sample, on the other hand, remains relatively constant with an increase in quercetin concentration from 0 to 50 μM. However, at a high

D
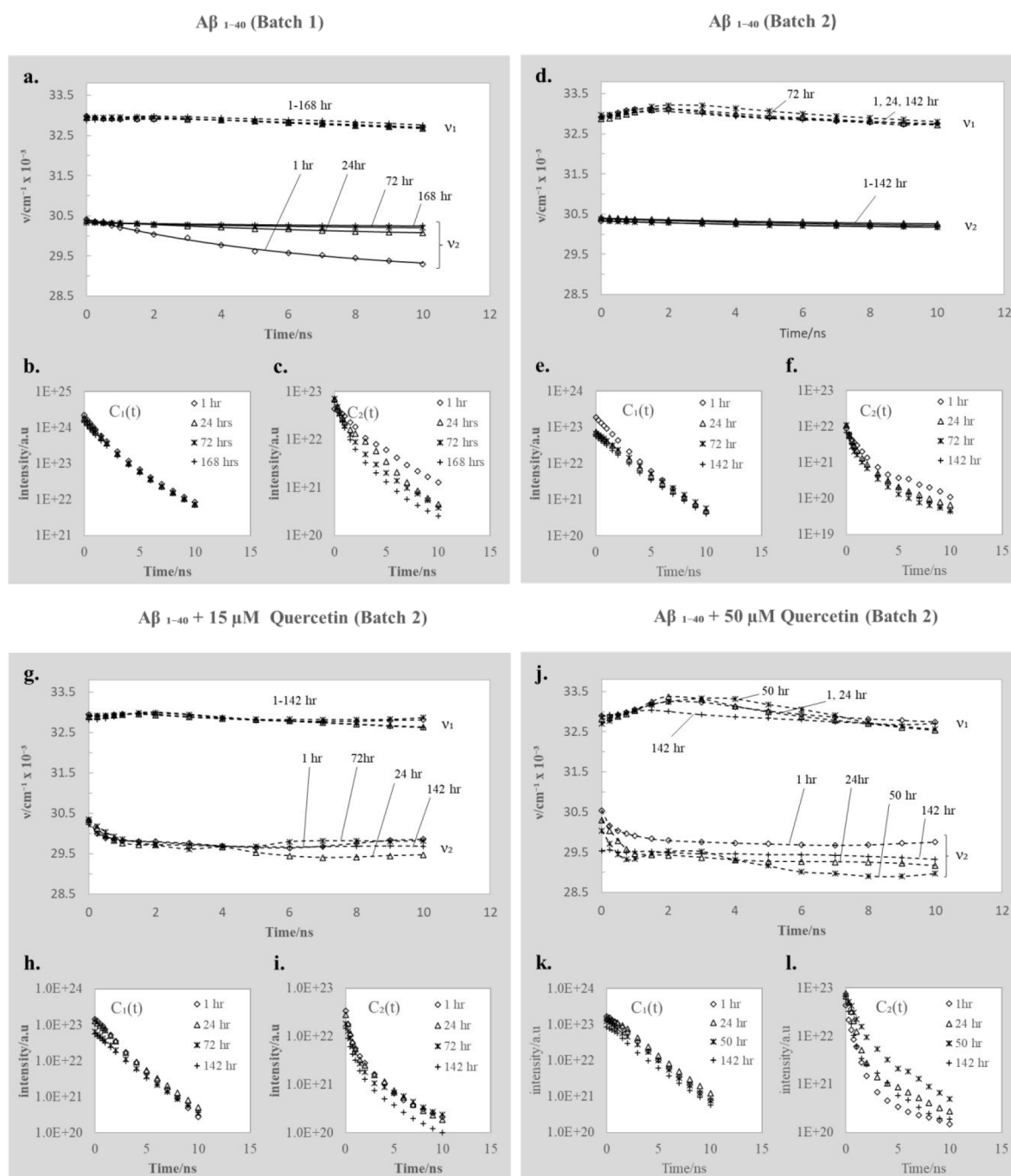
Figure 5. Peak positions $\nu_1(t)$ and $\nu_2(t)$ obtained from fitting Aβ_{1-40} TRES to eq 3, plotted against time in nanoseconds at different stages of aggregation for samples without (a, d) and with (g, j) quercetin. The fluorescence intensity decay of each component $C_1(t)$ and $C_2(t)$ obtained from fitting eq 3 to the experimental TRES data for the sample without (b, c, e, f) and with (h, i, k, l) quercetin.

concentration of quercetin, 200 μM, the emission of Aβ_{1-16} is considerably reduced (Figure 2b). The comparison of changes in the peak intensities for both Aβ fragments (Figure 2c) shows a gradual drop with an increase in quercetin concentration, suggesting inner filter effects due to quercetin absorption (Figure S3).

Fluorescence intensity decays of both Aβ_{1-11} and Aβ_{1-16} were best fitted to a 3-exponential model (Figure 3). The decay times τ_1, τ_2, and τ_3 and their *respective* percentage contributions f_1, f_2, and f_3 for Tyr in *both the* Aβ_{1-11} and Aβ_{1-16} samples showed no significant change with an increase in quercetin concentration. This indicates that the presence of quercetin does not impact

Tyr$_{10}$ fluorescence kinetics directly and confirms that the decrease in Aβ_{1-11} and Aβ_{1-16} emission intensity is due to the inner filter effect. To avoid this, quercetin in Aβ_{1-40} samples was kept at concentrations not exceeding 50 μM. Figure S4 also shows that quercetin (at 50 μM) does not have a direct effect on the intensity of Aβ_{1-40} emission (after 10 min) but surely has an effect on the aggregation process (after 24−142 h).

Aβ_{1-40} and Aβ_{1-40}-Quercetin Samples. TRES were obtained for a sample of Aβ_{1-40} in the absence of quercetin and in the presence of 15 and 50 μM of quercetin. Figure 4 shows TRES measured after 1 h and 142 h of incubation at 37 °C. The measurements obtained for the no-quercetin sample
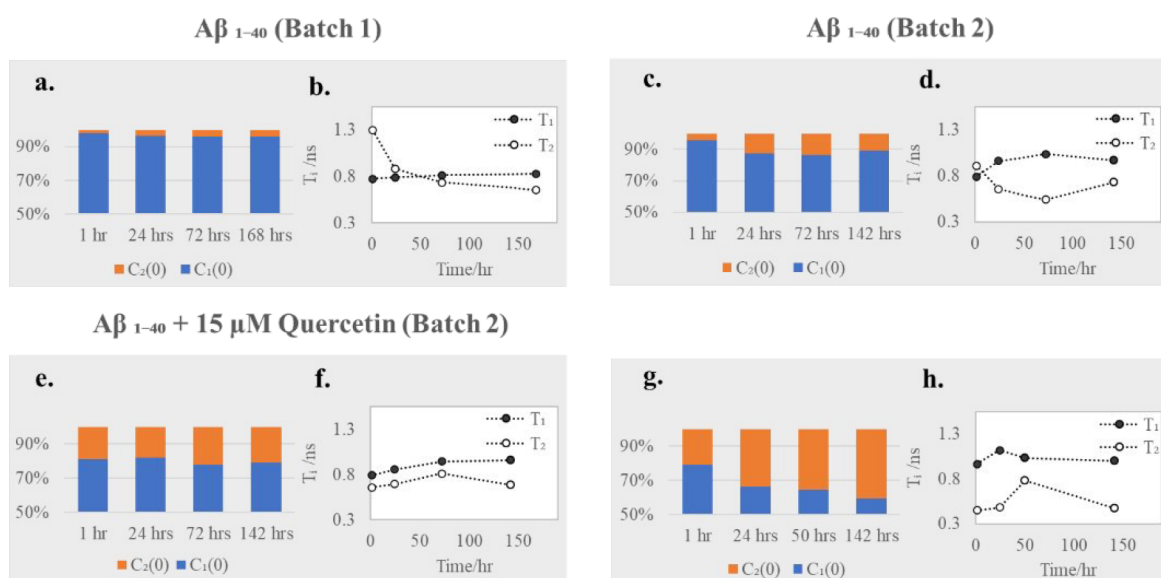
Figure 6. Initial percentage contribution of fluorescence intensity of the two emitting species, monomers $C_1(0)$ and oligomers $C_2(0)$ attained from fitting eq 3 to the measured TRES of $A\beta_{1-40}$ (batch 1) (a) and $A\beta_{1-40}$ (batch 2) in the absence (c) and the presence of two concentrations of quercetin 15 μM (e) and 50 μM (g). The characteristic fluorescence lifetimes of monomers T_1 and oligomers T_2 for $A\beta_{1-40}$ (batch 1) (b) and $A\beta_{1-40}$ (batch 2) in the absence (d) and presence of quercetin 15 μM (f) and 50 μM (h).

were first compared with the results obtained in our previous $A\beta_{1-40}$ TRES studies (batch 1).[24] The differences between the results for batch 1 and our current sample (batch 2) suggest that, in spite of applying the same sample preparation procedures in both cases (treatment by HFIP), batch 2 contains considerably more preformed aggregates. This demonstrates that the individual batches of even freshly purchased $A\beta_{1-40}$ material may not be identical in terms of the degree of aggregation and that the measurement of the "blank" sample needs to precede the measurements for the studied process and should be used as a reference. This also demonstrates the high sensitivity of our approach in establishing the stage of aggregation.

TRES of $A\beta_{1-40}$ in all samples were sufficiently represented by two peaks ($N = 2$) of the Toptygin-type function (3). The parameters recovered for all samples are plotted in Figure 5. We attribute the spectral peak values $\nu_1(t)$ to monomers and/or small oligomers, and $\nu_2(t)$ to larger oligomers.[24]

Note that the initial ($t = 0$) positions of all monomer peaks $\nu_1(t)$ are located at ~33000 cm^{-1}, and the initial ($t = 0$) positions of all oligomer peaks $\nu_2(t)$ are located at ~30500 cm^{-1}. These values are obtained mathematically when calculating the TRES data from the experimentally measured fluorescence decay, and importantly, they do not represent the energies of spectral maxima of the initial nonequilibrium Franck−Condon state of the excited tyrosine. Their shifts over 10 ns after excitation are highly influenced by the presence of $A\beta_{1-40}$ aggregates, the concentration of quercetin, and the age of the sample. The fluorescence intensity decay of each component is represented by the $C_1(t)$ and $C_2(t)$ functions obtained from fitting eq 3 to the experimental TRES data.

Here we discuss separately the results obtained in all four samples.

Free Ab$_{1-40}$ (Batch 1). The position of the peak $\nu_1(t)$ exhibits a very slow drop (Figure 5a). Indeed, in this case the $A\beta_{1-40}$ peptides are small in size and exposed to water molecules; thus, the dielectric relaxation process is fast and almost completed before fluorescence occurs. The position of $\nu_2(t)$ at 1 h after sample preparation, in the $A\beta_{1-40}$ sample free from aggregates

(Figure 5a), shifts exponentially from $\nu_2(0) \approx 30500$ cm^{-1} to $\nu_2(\infty) \approx 29000$ cm^{-1} with the dielectric relaxation time $\tau_R = 6.7$ ns. As the sample ages, the relaxation time τ_R increases, and the shift toward the red is reduced, due to the expected gradual growth in the size of the aggregates. We also note that the decay rate $C_1(t)$ is not affected by the age of the sample, which is natural considering that $C_1(t)$ represents monomers (Figure 5b), while the decay rates of the oligomers $C_2(t)$ (Figure 5c) are increasing with the age of the sample, reflecting more efficient quenching in larger aggregates.

Free Ab$_{1-40}$ (Batch 2). In the sample of partially aggregated peptides, the position of the peak $\nu_1(t)$ (Figure 5d) exhibits an initial shift toward higher wavenumbers followed by a shift toward lower wavenumbers. This behavior (also observed for $\nu_1(t)$ in the presence of quercetin, see Figure 5g,j) is unusual for the dielectric relaxation, and we believe that the $\nu_1(t)$ curves represent more than one form, most likely both monomers and very small oligomers, exhibiting slightly different fluorescence decay rates and relaxation times. The $\nu_2(t)$ (Figure 5d) exhibits a relatively small exponential shift with dielectric relaxation time $\tau_R = 8.7$ after 1 h of incubation. Again, the relaxation time τ_R increases with time of incubation, due to the growth of aggregates. Note that the behavior of $\nu_2(t)$ in Figure 5d is similar to that observed in Figure 5a at later times, suggesting that the processes in batch 2 were the same as in batch 1, but their monitoring started at the later stage of aggregation. Moreover, the decays $C_1(t)$ and $C_2(t)$ exhibit a change within 24 h only and then remain almost constant at later times (Figure 5e,f), which supports the above suggestion.

Ab$_{1-40}$ + 15 μM Quercetin (Batch 2). Adding 15 μM quercetin to the sample of $A\beta_{1-40}$ with existing aggregates (Figure 5g) has significantly changed the $\nu_2(t)$ behavior; it clearly shows a dielectric relaxation shift during the first 2 ns after excitation and then becomes constant. The curves are almost the same, when measured after 24, 72, and 142 h of incubation, suggesting that the aggregates formed might have reached stability much earlier than the free $A\beta_{1-40}$ aggregates. The presence of the solvatochromic shifts, which are not observed in

the free Aβ_{1-40} (batch 2) sample, suggests that quercetin forms complexes with Aβ_{1-40} peptides, and they are smaller than aggregates formed in the free Aβ_{1-40} samples at the same point in time during the aggregation process. Also, their formation prevents any further aggregation. The decays $C_1(t)$ and $C_2(t)$ are similar to those observed for free Ab$_{1-40}$ (batch 2) (Figure 5h,i).

Ab$_{1-40}$ + 50 µM Quercetin (Batch 2). At a higher quercetin concentration, the $\nu_2(t)$ dependence is modified further (Figure 5j). The evolution in $\nu_2(t)$ is nonexponential and is sensitive to the time of incubation. Clearly the model assuming two components is even more inadequate for the increased presence of quercetin. A more likely explanation is a variety of aggregates of different sizes, each exhibiting a distinct dielectric relaxation and fluorescence lifetime. The appearance of the solvatochromic shift suggests again that the Aβ_{1-40}-quercetin aggregates are smaller than the free Aβ_{1-40} aggregates at the same point in time. The lack of the shift in the position of $\nu_2(t)$ observed after 142 h of incubation suggests that the dielectric relaxation is finally blocked due to restricted rotational freedom of the environment surrounding tyrosine in large aggregates. At 50 µM of quercetin, the intensity decay of the first component $C_1(t)$ shows no significant changes, whereas $C_2(t)$ appears to be very sensitive to the age of the sample. The mean decay rate is not changing monotonically, which is likely to be caused by the variety of aggregate forms of different lifetimes and quantum yields, whose presence is changing during the aggregation process.

Further information on the effects of quercetin can be drawn out from the initial percentage contributions of fluorescence intensities of the two emitting species, monomers $C_1(0)$ and oligomers $C_2(0)$, and the fitted mean lifetimes T_1 and T_2, calculated from $C_1(t)$ and $C_2(t)$ curves (Figure 6).

After 1 h of incubation, 98% of fluorescence emission in batch 1 comes from monomers (Figure 6a), and as the sample ages, the percentage contribution of monomer $C_1(0)$ slightly decreases to about 95% indicating that monomers are aggregating and forming larger structures. $C_1(t)$ decays with a characteristic lifetime $T_1 \approx 0.8$ ns regardless of the sample's actual age (Figure 6b), which is consistent with $C_1(t)$ representing monomers. The characteristic lifetime T_2 of the decay $C_2(t)$ associated with oligomers decreases from 1.3 to 0.7 ns as the Aβ_{1-40} sample ages (Figure 6b), which may be explained by more intense quenching of fluorescence in larger aggregates.

In initially partially aggregated batch 2, the percentage contribution of monomers to fluorescence emission is reduced to about 95% after 1 h of incubation (Figure 6c) and continues to decrease with time of incubation until it reaches about 89% after 142 h. T_1 increases with time of incubation from 0.8 to about 1 ns (Figure 6d), while the initial value of T_2 is reduced to about 0.9 ns and continues to decrease over time (Figure 6d). This is an indication that the components $C_1(t)$ and $C_2(t)$ represent more than only two structures of distinct fluorescence lifetimes, which is consistent with the already mentioned unusual behavior of $\nu_1(t)$ (Figure 5d).

Adding 15 µM of quercetin to the Aβ_{1-40} sample reduces the initial contribution of monomers to about 80% after 1 h of incubation (Figure 6e). Increasing the quercetin concentration to 50 µM (Figure 6g) demonstrated further reduction in the contribution of monomers. In the presence of quercetin, both at the level of 15 and 50 µM, the T_1 behavior is similar (Figures.6f,h), suggesting that, as expected, the quercetin presence in the sample does not affect the monomers and smallest oligomers. Simultaneously, the initial value of T_2 is further reduced to 0.7 and 0.5 ns at concentrations 15 and 50

µM, respectively, due to increased Tyr quenching in larger aggregates.

To summarize the TRES analysis, parameters obtained from fitting eq 3 to the data collectively suggest that aggregation progresses differently in the presence of quercetin due to the formation of Aβ-quercetin complexes, which are likely to prevent further Aβ aggregation. The Aβ-quercetin complexes are not only different than aggregates without quercetin, but also are smaller, because formation of the big structures (which prevent dielectric relaxation) is hindered.

To examine further the stages of Aβ_{1-40} aggregation in the presence of quercetin, the process was monitored by the ThT binding assay in the absence and presence of 50 µM quercetin (Figure 7). Results show that Aβ_{1-40} starts forming β-sheet-rich
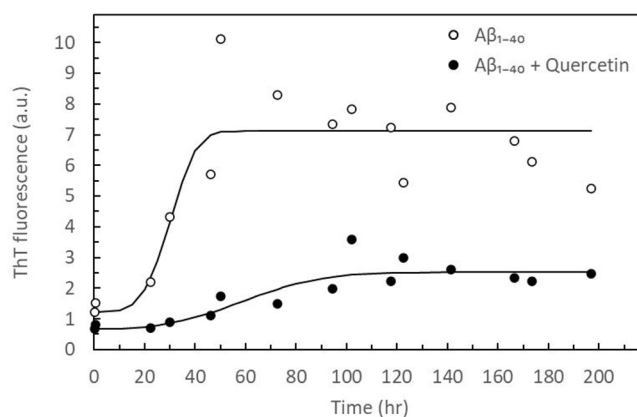
Figure 7. Time-dependent ThT fluorescence intensities measured at the peak ThT emission (484 nm) for 50 µM Aβ_{1-40} (batch 2) in the absence (○) and presence of 50 µM quercetin (●). The solid line is a guide to the eye.

aggregates after ∼24 h. A relatively rapid aggregation phase begins and, after ∼50 h, is followed by the saturation phase. Adding quercetin dramatically reduces the increase in ThT fluorescence, which can be explained by a much lower presence of β-sheet structures (thus prevented Aβ_{1-40} aggregation), providing that the potential quenching of ThT fluorescence by quercetin can be eliminated. Figure S5 shows that adding quercetin to a ThT solution does not reduce the ThT fluorescence; thus, no ThT quenching is observed. Therefore, the drop in ThT fluorescence in an Aβ_{1-40}-containing sample confirms that quercetin not only alters the aggregation pathways but also hinders formation of β-sheets.

◼ CONCLUSION

TRES measurements show a clear difference between the two batches of Aβ_{1-40}. We attribute this difference to the presence of preformed aggregates in the second batch. The presence of such aggregates affects the lag time for fibril formation. It may also have an impact on quercetin's ability to alter the aggregation pathway.

TRES data have also shown that the kinetics of Aβ_{1-40} aggregation in the presence of quercetin produces different fluorescent aggregates, as indicated by different changes in both peaks $\nu_1(t)$ and $\nu_2(t)$, with $\nu_2(t)$ showing dielectric relaxation. More interestingly, the fluorescence intensity contribution of the component $C_2(t)$ at $t = 0$ increases with quercetin concentration. This suggests an increase in the number oligomers, rather than an increase in their size. This is consistent

with the ThT binding assay confirming the lack of β-sheet structures. Thus, quercetin experiments show early formation of the Aβ-quercetin complexes, which seem to inhibit further Aβ aggregation. This fact, combined with quercetin being a natural nontoxic substance capable of crossing the blood–brain barrier, makes it a potential nutrient helping to prevent the onset and the development of Alzheimer's disease.

■ ASSOCIATED CONTENT

⑤ⓘ Supporting Information

The Supporting Information is available free of charge at https://pubs.acs.org/doi/10.1021/acs.jpcb.2c02763.

> Time-correlated single photon counting (TCSPC) measurements, TRES of Aβ_{1-40} at several stages of aggregation, absorption and emission spectra for tyrosine and quercetin, and emission spectra of Aβ_{1-40} (PDF)

■ AUTHOR INFORMATION

Corresponding Author

Olaf J. Rolinski − *Photophysics Group, Centre for Molecular Nanometrology, Department of Physics, Scottish Universities Physics Alliance, University of Strathclyde, Glasgow G4 0NG, United Kingdom;* ⊙ orcid.org/0000-0002-7838-779X; Email: o.j.rolinski@strath.ac.uk

Authors

Abeer Alghamdi − *Photophysics Group, Centre for Molecular Nanometrology, Department of Physics, Scottish Universities Physics Alliance, University of Strathclyde, Glasgow G4 0NG, United Kingdom*

David J.S. Birch − *Photophysics Group, Centre for Molecular Nanometrology, Department of Physics, Scottish Universities Physics Alliance, University of Strathclyde, Glasgow G4 0NG, United Kingdom*

Vladislav Vyshemirsky − *School of Mathematics and Statistics, University of Glasgow, Glasgow G12 8QQ, United Kingdom*

Complete contact information is available at:
https://pubs.acs.org/10.1021/acs.jpcb.2c02763

Notes

The authors declare no competing financial interest.

■ ACKNOWLEDGMENTS

■ REFERENCES

(1) Ferrer, J. L.; Austin, M. B.; Stewart Jr, C.; Noel, J. P. Structure and function of enzymes involved in the biosynthesis of phenylpropanoids. *Plant Physiol. Biochem.* **2008**, *46*, 356−370.

(2) Jan, S.; Abbas, N. *Himalayan Phytochemicals: Sustainable Options for Sourcing and Developing Bioactive Compounds*; Elsevier, 2018.

(3) Kay, C.; Cassidy, A. *Encyclopedia of Human Nutrition: Phytochemicals: Classification and Occurrence* **2013**, 490−497.

(4) Pastor-Villaescusa, B.; Rodriguez, E. S.; Rangel-Huerta, O. D. Polyphenols in obesity and metabolic syndrome. *Obesity*; Academic Press, 2018; pp 213−239.

(5) Di Matteo, V.; Pierucci, M.; Di Giovanni, G.; Esposito, E. Prevention and therapy of neurodegenerative disorders: role of nutritional antioxidants. In *Oxidative Stress and Neurodegenerative Disorders*; Elsevier Science BV, 2007; pp 621−661.

(6) Lesjak, M. M.; Beara, I. N.; Orčić, D. Z.; Petar, K. N.; Simin, N.Đ.; Emilija, S.Đ.; Mimica-Dukić, N. M. Phytochemical composition and antioxidant, anti-inflammatory and antimicrobial activities of Juniperus macrocarpa Sibth. et Sm. *J. Funct. Foods* **2014**, *7*, 257−268.

(7) Echeverría, F.; Ortiz, M.; Valenzuela, R.; Videla, L. A. Hydroxytyrosol and cytoprotection: A projection for clinical interventions. *Int. J. Mol. Sci.* **2017**, *18* (5), 930.

(8) Molina, M. F.; Sanchez-Reus, I.; Iglesias, I.; Benedi, J. Quercetin, a flavonoid antioxidant, prevents and protects against ethanol-induced oxidative stress in mouse liver. *Biol. Pharm. Bull.* **2003**, *26*, 1398−1402.

(9) Leopoldini, M.; Russo, N.; Chiodo, S.; Toscano, M. Iron chelation by the powerful antioxidant flavonoid quercetin. *J. Agric. Food Chem.* **2006**, *54*, 6343−6351.

(10) Kim, H.; Park, B. S.; Lee, K. G.; Choi, C. Y.; Jang, S. S.; Kim, Y. H.; Lee, S. E. Effects of naturally occurring compounds on fibril formation and oxidative stress of β-amyloid. *J. Agric. Food Chem.* **2005**, *53*, 8537−8541.

(11) DeTure, M. A.; Dickson, D. W. The neuropathological diagnosis of Alzheimer's disease. *Mol. Neurodegener.* **2019**, *14*, 32.

(12) Schelle, J.; Häsler, L. M.; Göpfert, J. C.; Joos, T. O.; Vanderstichele, H.; Stoops, E.; Mandelkow, E. M.; Neumann, U.; Shimshek, D. R.; Staufenbiel, M.; et al. Prevention of tau increase in cerebrospinal fluid of APP transgenic mice suggests downstream effect of BACE1 inhibition. *Alzheimer's Dement.* **2017**, *13*, 701−709.

(13) Israel, M.; Yuan, S. H.; Bardy, C.; Reyna, S. M.; Mu, Y.; Herrera, C.; Hefferan, M. P.; Van Gorp, S.; Nazor, K. L.; Boscolo, F.S.T A.; et al. Probing sporadic and familial Alzheimer's disease using induced pluripotent stem cells. *Nature* **2012**, *482*, 216−220.

(14) Choi, S. H.; Kim, Y. H.; Hebisch, M.; Sliwinski, C.; Lee, S.; D'Avanzo, C.; Chen, H.; Hooli, B.; Asselin, C.; Muffat, J.; et al. A three-dimensional human neural cell culture model of Alzheimer's disease. *Nature* **2014**, *515*, 274−278.

(15) Lee, H. K.; Velazquez Sanchez, C.; Chen, M.; Morin, P. J.; Wells, J. M.; Hanlon, E. B.; Xia, W. Three dimensional human neuro-spheroid model of Alzheimer's disease based on differentiated induced pluripotent stem cells. *PLoS One* **2016**, *11*, No. e0163072.

(16) Maia, L. F.; Kaeser, S. A.; Reichwald, J.; Hruscha, M.; Martus, P.; Staufenbiel, M.; Jucker, M. Changes in amyloid-β and Tau in the cerebrospinal fluid of transgenic mice overexpressing amyloid precursor protein. *Sci. Transl. Med.* **2013**, 5, 194re2.

(17) Oddo, S.; Caccamo, A.; Shepherd, J. D.; Murphy, M. P.; Golde, T. E.; Kayed, R.; Metherate, R.; Mattson, M. P.; Akbari, Y.; LaFerla, F. M. Triple-transgenic model of Alzheimer's disease with plaques and tangles: intracellular Aβ and synaptic dysfunction. *Neuron* **2003**, *39*, 409−421.

(18) Heijnen, C. G. M.; Haenen, G. R. M. M.; Minou Oostveen, R.; Stalpers, E. M.; Bast, A. Protection of flavonoids against lipid peroxidation: the structure activity relationship revisited. *Free Radic. Res.* **2002**, *36*, 575−581.

(19) Zaplatic, E.; Bule, M.; Shah, S. Z. A.; Uddin, M. S.; Niaz, K. Molecular mechanisms underlying protective role of quercetin in attenuating Alzheimer's disease. *Life Sci.* **2019**, *224*, 109−119.

(20) Porat, Y.; Abramowitz, A.; Gazit, E. Inhibition of amyloid fibril formation by polyphenols: structural similarity and aromatic inter-actions as a common inhibition mechanism. *Chem. Biol. Drug Des.* **2006**, *67*, 27−37.

(21) Wang, J.-B.; Wang, Y.-M.; Zeng, C.-M. Quercetin inhibits amyloid fibrillation of bovine insulin and destabilizes preformed fibrils. *Biochem. Biophys. Res. Commun.* **2011**, *415*, 675−679.

(22) Zhu, M.; Han, S.; Fink, A. L. Oxidized quercetin inhibits α-synuclein fibrillization. *Biochim. Biophys. Acta (BBA)-General Subj.* **2013**, *1830*, 2872−2881.

(23) Jiménez-Aliaga, K.; Bermejo-Bescós, P.; Benedí, J.; Martín-Aragón, S. Quercetin and rutin exhibit antiamyloidogenic and fibril-disaggregating effects in vitro and potent antioxidant activity in APPswe cells. *Life Sci.* **2011**, *89*, 939−945.

(24) Alghamdi, A.; Vyshemirsky, V.; Birch, D. J. S.; Rolinski, O. J. Detecting beta-amyloid aggregation from time-resolved emission spectra. *Methods Appl. Fluoresc.* **2018**, *6*, 024002.

(25) Chen, G.; Xu, T. H.; Yan, Y.; Zhou, Y. R.; Jiang, Y.; Melcher, K.; Xu, H. E. Amyloid beta: structure, biology and structure-based therapeutic development. *Acta Pharmacol. Sin.* **2017**, *38*, 1205−1235.

(26) Srivastava, A.; Singh, P. K.; Kumbhakar, M.; Mukherjee, T.; Chattopadyay, S.; Pal, H.; Nath, S. Identifying the bond responsible for the fluorescence modulation in an amyloid fibril sensor. *Chem.—Eur. J.* **2010**, *16*, 9257−9263.

(27) Stsiapura, V. I.; Maskevich, A. A.; Kuzmitsky, V. A.; Uversky, V. N.; Kuznetsova, I. M.; Turoverov, K. K. Thioflavin T as a molecular rotor: fluorescent properties of thioflavin T in solvents with different viscosity. *J. Phys. Chem. B* **2008**, *112*, 15893−15902.

(28) Younan, N. D.; Viles, J. H. A comparison of three fluorophores for the detection of amyloid fibers and prefibrillar oligomeric assemblies. ThT (thioflavin T); ANS (1-anilinonaphthalene-8-sulfonic acid); and bisANS (4, 4′-dianilino-1, 1′-binaphthyl-5, 5′-disulfonic acid). *Biochemistry* **2015**, *54*, 4297−4306.

(29) Broersen, K.; Jonckheere, W.; Rozenski, J.; Vandersteen, A.; Pauwels, K.; Pastore, A.; Rousseau, F.; Schymkowitz, J. A standardized and biocompatible preparation of aggregate-free amyloid beta peptide for biophysical and biological studies of Alzheimer's disease. *Protein Eng. Des. Sel.* **2011**, *24*, 743−750.

(30) Stine, W. B.; Dahlgren, K. N.; Krafft, G. A.; LaDu, M. J. In vitro characterization of conditions for amyloid-β peptide oligomerization and fibrillogenesis. *J. Biol. Chem.* **2003**, *278*, 11612−11622.

(31) Mcguinness, C. D.; Sagoo, K.; Mcloskey, D.; Birch, D. J. S. A new sub-nanosecond LED at 280 nm : *Meas. Sci. Technol.* **2004**, *15*, L19−22.

(32) Rolinski, O. J.; McLaughlin, D.; Birch, D. J. S.; Vyshemirsky, V. Resolving environmental microheterogeneity and dielectric relaxation in fluorescence kinetics of protein. *Methods Appl. Fluoresc.* **2016**, *4*, 024001.

(33) Rolinski, O. J.; Wellbrock, T.; Birch, D. J. S.; Vyshemirsky, V. Tyrosine photophysics during the early stages of β-amyloid aggregation leading to Alzheimer's. *J. Phys. Chem. Lett.* **2015**, *6*, 3116−3120.

(34) Toptygin, D.; Brand, L. Spectrally-and time-resolved fluorescence emission of indole during solvent relaxation: a quantitative model. *Chem. Phys. Lett.* **2000**, *322*, 496−502.

📖 Recommended by ACS